Controls on Evaporation in a Boreal Spruce Forest

ALAN K. BETTS
Pittsford, Vermont

MIKE GOULDEN
Earth System Science, University of California, Irvine, Irvine, California

STEVE WOFSY
Division of Engineering and Applied Science, Harvard University, Cambridge, Massachusetts

(Manuscript received 4 March 1998, in final form 19 June 1998)

ABSTRACT

The surface energy balance over a boreal spruce forest is analyzed using 3 yr of 30-min-averaged data collected during the 1994–96 Boreal Ecosystem–Atmosphere Study experiment 40 km west of Thompson, Manitoba, to show the climatic controls on surface evapotranspiration. The seasonal variation of evaporation is shown: lowest in spring when the ground is frozen, highest in summer (although daytime evaporative fractions are only 0.4), and lower again in fall after frost. The surface sensible heat flux in contrast is high in spring, when evaporation is low. Evaporation is much higher when the surface, including the moss layer, is wet. At all temperatures (in summer), evaporative fraction falls with increasing light level, because of the high vegetative resistance of the forest system. Using a Monin–Obukhov formulation and a bulk vegetation model, the vegetative resistance for the boreal spruce forest system is calculated. This bulk vegetative resistance decreases with increasing photosynthetic radiation, decreases sharply with relative humidity, decreases with increasing surface water storage, and is lower on cloudy days than on sunny days with the same incoming photosynthetic radiation. Vegetative resistance at its midmorning minimum is lower by a factor of 4 when the moss surface is very wet. As over grassland sites, the lower surface resistance to evaporation directly influences the diurnal cycle of lifting condensation level and cloud-base height, which are much lower on days with a wet surface. The reduction of vegetative resistance under cloudy skies at the same incoming radiation level presumably reflects the more efficient use of diffuse radiation by the canopy for photosynthesis. Vegetative resistance is roughly doubled in spring, when the ground is frozen, and is higher in fall after frost. About 63% of the observed variance in vegetative resistance can be explained in terms of meteorological variables using multiple linear regression. Some measurement issues are addressed in an appendix. The residual in the energy balance falls with increasing wind speed, which may be due to a small (10%–15%) underestimation of the sensible and latent heat fluxes at low wind speeds. During spring melt, however, this residual has a high daytime value of 30% of net radiation. The residual is also much higher on sunny days than on cloudy days.

1. Introduction

The surface energy balance, in particular the partition of the net radiation at the surface into the sensible and latent heat fluxes, plays a key role in influencing weather and climate over land on both diurnal and seasonal timescales. In current global forecast and climate models, this land surface boundary condition is computed using many submodels (e.g., for the subsurface hydrology, vegetation, surface and boundary layers, radiation, and clouds). Despite improvements in many of these components in recent years, global forecast models still suffer from errors in their land surface parameterizations (e.g., Betts et al. 1996, 1998a,b). These errors introduce systematic biases in the model climatology that are one factor limiting medium-range and seasonal forecast skill and our ability to model the present-day climate. Improvements in the representation of the land surface boundary condition have shown clear improvements in model forecast skill (e.g., Beljaars et al. 1996). From a climatic perspective, two key factors are important. The first is the surface radiation budget, which is determined by season, latitude, atmospheric aerosol, and cloud cover, as well as the surface albedo. The second is the partition of the net radiation minus ground heat flux into the sensible and latent heat fluxes to the atmosphere, which is controlled over land by the availability of water

Corresponding author address: Dr. Alan K. Betts, 58 Hendee Ln., Pittsford, VT 05763.
E-mail: akbetts@aol.com

for evaporation, and the biophysical controls on transpiration. The high-latitude boreal forests have a very low surface albedo in summer, around 0.08–0.09, and rather low values in winter, typically <0.2 (Betts and Ball 1997), since the canopy shades the snow from the low elevation angle solar insolation. This paper focuses on the second factor: the controls on forest evaporation that can be inferred from a long observational record.

Only recently have long-term eddy covariance flux measurements become feasible (Wofsy et al. 1993), which permits the seasonal study of the surface energy balance and gas exchange at the surface. This provides an observational basis for the study of the important physical processes at the land surface. In this paper we continue the analysis of one of the first of these datasets, a two and one-half-year record over a boreal forest. During the Boreal Ecosystem–Atmosphere Study (BOREAS), eddy covariance measurements of the fluxes of momentum, sensible heat (SH), latent heat (LH), and CO_2 were made over the boreal forest in Saskatchewan and Manitoba in Canada. This paper analyzes the energy and water fluxes from March 1994 to October 1996 from one site, the BOREAS northern study area (NSA) old black spruce site (NSA-OBS) 40 km west of Thompson, Manitoba (55.879°N, 98.484°W; Sellers et al. 1995), over a stand of black spruce [*Picea mariana* (Mill.) BSP] forest. Similar measurements were made at a second black spruce site 100 km north of Prince Albert in Saskatchewan (Jarvis et al. 1997; Pattey et al. 1997). This is a common forest over the North American boreal zone (Larson 1980). Our objective is to explore the observed dependence of evaporation and a bulk estimate for vegetative resistance on key measured quantities, such as air and soil temperature, soil moisture, humidity, wind speed, incoming solar radiation, cloudiness, and precipitation. Our simplified surface model framework (section 2) is similar to that used in global forecast models, like that at European Centre for Medium-Range Weather Forecasts (ECMWF). This is a deliberate choice since we wish to provide guidance for improving global forecast and climate models for the boreal regions. Errors in the surface energy balance over the boreal forest (which is circumpolar) lead to large systematic model errors in the Northern Hemisphere, which are particularly large in spring (Betts et al. 1998b).

a. Overview of the flux data

In the past few years more than 50 long-term flux sites have been installed around the world, primarily over forests. These are providing a wealth of data on the land surface interaction over different ecosystems. Since this analysis is one of the first looking at several years of this flux data from a hydrometeorological and climatic perspective, we believe the reader should understand some of the observational issues. The fluxes measured from a long-term forest site are representative of only a small area (<1 km^2), and all measurements are subject to particular instrumental errors, which are discussed in the references and to a limited extent in the appendix. This measurement site was very level, with black spruce forest of varying stature for several kilometers in all directions. The vegetation immediately around the site differed markedly with small changes in elevation. Upland areas were dominated by dense, 10-m-tall, 120-yr-old black spruce with a minor shrub layer and continuous feather moss. Low-lying areas were dominated by sparse, 1-to-6-m-tall, chlorotic spruce and continuous sphagnum moss. Approximately 90% of the area within 500 m of the tower was black spruce forest, 45% had underlying feather moss, and 45% sphagnum moss, and the remaining 10% of the area was fen (Harden et al. 1997). Boardwalks around the site minimized disturbance, and access to areas south, west, and north of the tower was strictly limited. The data acquisition and control systems were fully automated, allowing extended periods of unattended operation. The turbulent fluxes of SH, LH, CO_2, and momentum at 29 m were determined following Wofsy et al. (1993) and Goulden et al. (1996a,b), and the details of the data processing are given in Goulden et al. (1997). In their analysis, Goulden et al. (1997) excluded wind directions from behind the tower (45°–135°); however, we found that the impact of excluding these data was small, so we decided to include all wind directions in this paper. The photosynthetically active photon flux density (PPFD) above the forest was measured with a silicon quantum sensor, and moss-surface PPFD was measured at eight locations along a topographic gradient. The net radiation at 29 m was measured with a thermopile net radiometer. Air temperatures at 1-, 8-, and 28-m altitude were measured with ventilated thermistors. Soil temperatures at 5, 10, 20, 50, and 100 cm beneath the moss surface were measured at five sites along a topographic gradient with precision thermistors. In this paper we have used an average of the 10-cm soil temperature for two sites, one with feather and one with sphagnum moss.

For the second half of the measurement period (13 July 1995 onward) we have at five levels (7.5, 22.5, 45, 75, and 105 cm below the *base* of the moss layer) soil moisture measurements from an array of eight time domain reflectometry (TDR) rods on a radial line away from the flux tower (Cuenca et al. 1997). These TDR rods start approximately 20 m from the tower and are then spaced approximately every 10 m. The soil at the site is stratified with the upper two measurements generally in the organic layer (below the moss layer) and the lower three in the underlying clay layer. We generated daily average values of soil moisture for the 0–30-cm organic layer, representative of the spruce root zone. Volumetric soil moisture values are high, generally in the range 0.4–0.7. Previous studies over grassland (e.g., Smith et al. 1992; Verma et al. 1992; Betts and Ball 1995, 1998) have shown the important role of soil moisture in controlling evapotranspiration and

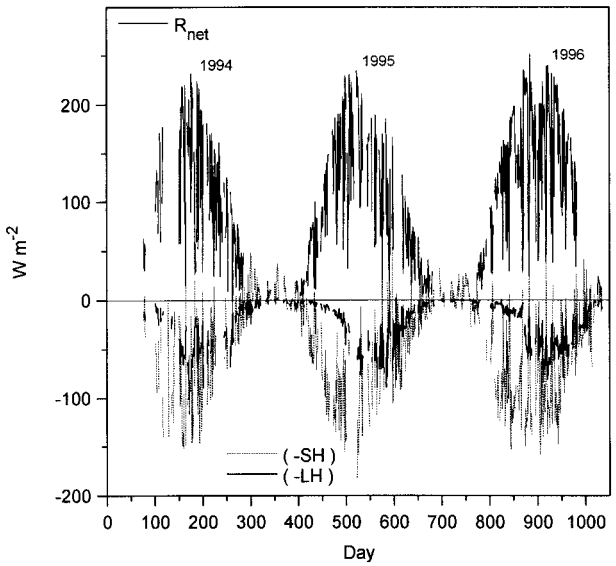

FIG. 1. Daily averages of R_{net}, SH, and LH for the 3 yr 1994–96. Day 1 is 1 Jan 1994.

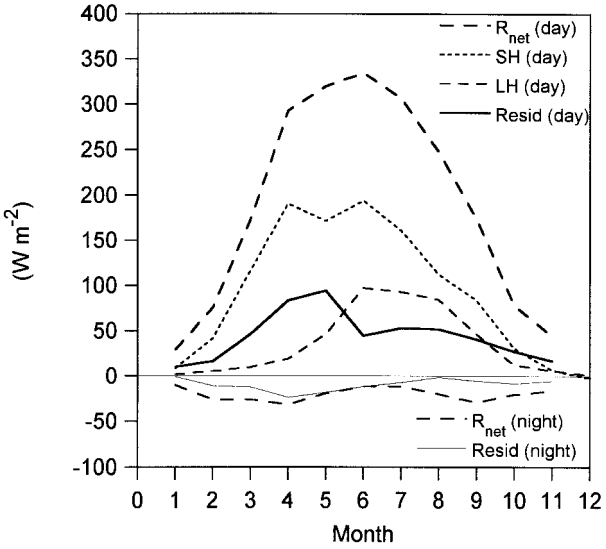

FIG. 2. Annual cycle of terms in the surface energy balance.

therefore the land surface boundary condition; however, we shall show that for the wet organic soils of this black spruce forest, soil water variations though considerable have no detectable effect of evaporation.

In this study we use 30-min segments of data from March 1994 to October 1996. There are some gaps when key parts of the automated system malfunctioned, but there are a total of 23 000 h of data. Figure 1 shows a summary of the available data showing the seasonal cycle of SH, LH, and net radiation (R_{net}) for the three years 1994–96. The data are daily average values and days of incomplete data are omitted. Day zero is 1 January 1994, and for visual convenience we have reversed the sign on SH and LH (in this figure only). Although the seasonal cycle of R_{net} is roughly symmetric about the summer solstice, the seasonal cycles of SH and LH are very different and asymmetric (although they are similar from year to year). Sensible heat is very high and LH is very low in spring, while in the fall SH and LH are comparable in magnitude. The reason is the large seasonal lag of the soil temperatures at these high latitudes. In spring, the soil at 10-cm depth melts at this site in the middle of May (days 144, 493, and 875 on Fig. 1). Before soil melt LH is very low, because water is not available for evapotranspiration. In the fall, the soil does not start to freeze (from the surface) until late October, and the soil at 50 cm does not freeze until December, so water remains available for evapotranspiration until radiation levels are very low (although after frost, canopy photosynthesis and transpiration are reduced). Our analysis will focus primarily on a subset of the data, the daytime unstable surface layer, with an emphasis on the summer growing season, after soil melt and before the first frost. We will also show, however, the impact of frozen soil and the spring transition on the surface fluxes, and the somewhat smaller impact of frost in the fall. Our technique will be to show composites of the 30-min data averages, stratified by different variables, to illustrate the key dependencies that are visible in these 3 yr of data for the forest ecosystem.

The closure of the *surface energy budget* is one overall indicator of the accuracy of the flux measurements. However, we have no accurate measurements of ground heat flux, as the heat flux plates did not survive the first winter. Goulden et al. (1997) discussed the residual (Resid) in the surface energy budget, calculated as

$$\text{Resid} = R_{net} - \text{SH} - \text{LH}. \quad (1)$$

They commented that Resid/R_{net} = 0.18 on average, and this ratio reached a maximum in spring, when energy was used for the melt of soil and snow. Figure 2 shows the seasonal cycle of daytime (a 1200–2400 UTC mean) R_{net}, SH, LH, and the residual (heavy solid line), and the nighttime R_{net} and residual (a 0000–1200 UTC mean). All the data has been simply binned into months. There is a sharp fall in the daytime residual between May and June coinciding with the end of snow and soil melt. Simultaneously, the daytime LH flux rises after soil melt, coinciding with the increase in plant photosynthetic activity, while SH rises much earlier in spring, when R_{net} is high and evaporation low. At night the residual is comparable to the measured SH flux (not shown), while the measured LH flux at night is small and upward (not shown). We have less confidence in the flux measurements at night, especially when wind speeds are low, and this analysis will exclude them. Figure 3 shows the diurnal cycle of Resid in 3-h averages for April–July, 4 months for which R_{net} has closely similar peaks of around 430 W m^{-2}.

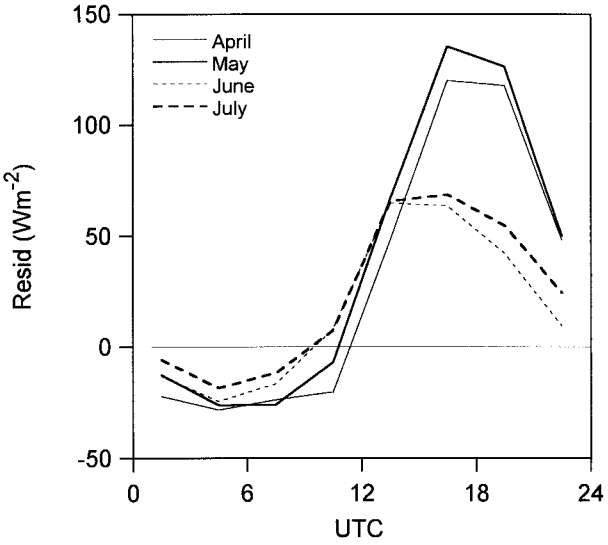

FIG. 3. Diurnal cycle of Resid in surface energy balance from Apr to Jul.

The residual is much higher in April and May, when the snow and surface is melting and energy is going into the phase change; for this period the daytime average of Resid/R_{net} = 0.29. In June and July, after the ground has melted, the daytime residual falls dramatically, and the daytime average of Resid/R_{net} is halved to 0.15. At night however the residual exceeds 50% of R_{net} and the accuracy of the flux measurements is more uncertain. A more detailed analysis of the energy budget residual, in particular its dependence on wind speed, soil melt, and cloud cover, is given in the appendix. This paper will focus mainly on daytime fluxes, after ground thaw, when the energy budget residual is small, and our confidence in the SH and LH flux measurements is correspondingly higher.

b. Links between transpiration and photosynthesis

Our analysis focuses on linking the forest energy and water fluxes to surface and atmospheric variables. We will calculate a bulk ''vegetative resistance'' (the reciprocal of a conductance) from measured evaporation and a near-surface meteorological model. From a climatic perspective, it is this additional resistance to evaporation at the surface that distinguishes the land surface from the ocean, and gives the deeper, drier boundary layers seen over land (see Fig. 9c later).

There has been much research on the underlying physiological processes that link transpiration to photosynthesis. The stomatal conductance of plants is known to exert a major control on the evaporation from tall vegetation (Jarvis and McNaughton 1986). The mechanisms that determine stomatal response to the environment remain incompletely understood despite a century of research (Monteith 1995). Nonetheless, it is widely recognized that the stomata of individual species respond to light, CO_2, evaporative demand, and soil drought in predictable ways, and that these responses are consistent across a range of species (Jones 1992). As a result, a large number of empirical models, directly linking conductance to photosynthesis, have been presented and used to predict evaporation for ecological, agronomic, hydrological, or meteorological applications (Jarvis 1976; Collatz et al. 1991; Jones 1992; Leuning 1995). This paper does not address these links to photosynthesis, although we plan to explore them later. However, Goulden et al. (1997), using this same dataset, have already analyzed the CO_2 exchange between the atmosphere and the black spruce forest from a physiological perspective, and we will briefly summarize their results. The eddy covariance method only measures the net CO_2 exchange, but gross photosynthetic uptake can be found by subtracting forest respiration. Goulden et al. (1997) estimated daytime respiration using simple temperature-dependent exponential formulas fitted to the CO_2 flux measurements at higher wind speeds at night, when photosynthesis is zero. They found that photosynthetic uptake varied seasonally, with no photosynthesis observed in winter. A rapid recovery of photosynthetic capacity was observed with warming in spring, and photosynthesis responded in a consistent manner to weather throughout the summer. Photosynthesis at high light was negligible at $T_{air} < 0$°C, increased linearly with T_{air} from 0°C to 14°C, and was relatively insensitive to $T_{air} > 14$°C. Photosynthesis at $T_{air} > 14$°C increased with increasing light before saturating at incident PPFD greater than 500–700 μmol m^{-2} s^{-1}. Photosynthesis in summer did not appear limited by high evaporative demand or soil water depletion. They also found that photosynthesis was higher at the same incoming radiation level under cloudy skies than in direct sunlight.

Qualitatively we would therefore expect evaporation from the forest system to have somewhat similar dependencies on environmental variables as photosynthesis, increasing with increasing light level and under cloudy skies, for example. However we shall also find that the evaporation from the surface moss layer when wet, which is not photosynthetically controlled, is important climatically. The negative feedback between environmental RH and evaporation appears to be large and it will be explored in detail.

2. Modeling framework

We shall interpret the 3 yr of 30-min mean flux data from this old black spruce site using a Monin–Obukhov similarity framework and a simple bulk surface model, with a single vegetation parameter, a bulk vegetative resistance for the forest ecosystem. This is characteristic of the level of complexity of the land surface model in current global forecast models, such as that at the European Centre for Medium-Range Weather Forecasts

(ECMWF) and the National Centers for Environmental Prediction (NCEP). More complex models exist, such as the biosphere–atmosphere scheme (Dickinson et al. 1986) and the simple biosphere model (Sellers et al. 1986) and are in widespread use in global climate models. However, because of their greater complexity, it is correspondingly more difficult to derive their more extensive parameter sets from observations, such as the ones we have here. All forecast and climate models distinguish evaporation from bare ground, wet canopy, and transpiration from the vegetation. In the boreal spruce forest the fraction of bare ground is small, as the surface has a widespread moss cover, and we will be able to show that the moss layer plays an important role in the surface hydrology. We were not able however to separate the effect of a wet canopy from wet moss in our analysis. The bulk of the data we shall analyze is however on days without rain, when the canopy is likely to be dry.

Our focus will be to explore the *observed* dependencies of this single bulk vegetative resistance on air and soil temperature, humidity, wind speed, incoming photosynthetic radiation, soil moisture, and on two indices related to cloud cover and the wetness of the surface, which will be defined later. This provides an observational basis for understanding the coupling between atmospheric parameters and the evapotranspiration from the forest, and consequently possible feedbacks of the land surface on climate. In a later paper we will compare these observed dependencies of vegetative resistance, derived from the BOREAS data, with those in model formulations.

a. Surface flux framework

We use the bulk aerodynamic equations with aerodynamic and vegetative conductances. For momentum

$$u_*^2 = g_M U, \tag{2}$$

where u_* and U are the surface friction velocity and mean scalar wind speed, which are measured, and g_M is an aerodynamic conductance for momentum. We will use this equation to estimate surface roughness using the Monin–Obukhov formulation in section 2b. For the measured SH heat flux, we use

$$\mathrm{SH}/\rho C_p = u_*\theta_* = g_H(T_c - T_{\mathrm{air}}), \tag{3}$$

where T_c is an aerodynamic temperature (for the canopy, which is not measured), T_{air} is the measured air temperature (at 29 m), and θ_* is the temperature scale. The aerodynamic conductance for heat is g_H, and this will also be calculated from the Monin–Obukhov formulation.

For water vapor, the LH flux is measured and we add a single vegetative conductance g_{veg}, for the entire forest system, and assume the same aerodynamic conductance as for heat, and saturation q_s at temperature T_c:

$$\mathrm{LH}/\rho L = \left(\frac{g_H g_{\mathrm{veg}}}{g_H + g_{\mathrm{veg}}}\right)[q_s(T_c) - q_{\mathrm{air}}], \tag{4a}$$

$$= [q_s(T_c) - q_{\mathrm{air}}]/(R_H + R_{\mathrm{veg}}), \tag{4b}$$

where resistances have been defined as

$$R_{\mathrm{veg}} = 1/g_{\mathrm{veg}}; \qquad R_H = 1/g_H. \tag{5}$$

The aerodynamic resistance R_H is very much smaller (mean value in our dataset of 10 s m^{-1}) than R_{veg} (mean value of 330 s m^{-1} when the surface is dry). Note that we have assumed a single aerodynamic temperature for the canopy, T_c in (3), as well as saturation at this temperature in (4), along with the single vegetative conductance or resistance. This is the ''big-leaf'' idealization of the whole forest system. Its main limitation is that we are combining different evaporative processes since we cannot split the measured LH flux into its separate components. Evapotranspiration from the vegetation is subject to stomatal control, while evaporation from wet surfaces (which in the spruce forest includes the moss understory) is not. In, for example, the ECMWF global model, while a big-leaf model is used for evapotranspiration, a separate calculation of evaporation is made for a wet skin reservoir, although a single surface temperature is assumed.

The computational procedure is to calculate g_H from the Monin–Obukhov model, then derive from (3) the canopy aerodynamic temperature, T_c, which is an unknown as it is not measured. Then (4) can be solved for g_{veg} or R_{veg}, using a calculated $q_s(T_c)$, the measured surface SH and LH fluxes, and the measured T_{air} q_{air} at 29 m.

b. Monin–Obukhov surface model

We use the formulation from Beljaars and Holtslag (1991) because it is used in the ECMWF model. For wind and the momentum flux,

$$\frac{U}{u_*} = \frac{1}{k}\left[\ln\left(\frac{Z - D}{Z_{\mathrm{OM}}}\right) - \Psi_M\left(\frac{Z - D}{L_v}\right)\right]. \tag{6}$$

where $k = 0.4$ is the von Kármán constant, $Z = 29$ m is the measurement height, D a displacement height, and Z_{OM} the surface roughness. The Monin–Obukhov length, L_v, was calculated from the measured surface fluxes as

$$L_v = \frac{\theta_v u_*^2}{kg\theta_{v*}Z} \tag{7}$$

using the virtual heat flux ($u_*\theta_{v*}$), and the Monin–Obukhov ψ_M function is defined below. The canopy height was 10 m (Goulden et al. 1997), so we used a value for the displacement height D of 5 m. We then solved (6) to obtain a mean value of

$$\frac{1}{k}\ln\left(\frac{Z - D}{Z_{\mathrm{OM}}}\right) = 7.75, \tag{8}$$

giving a roughness height $Z_{OM} = 1.08$ m for $Z - D = 29 - 5 = 24$ m. At 11% of the canopy height this is a reasonable value for Z_{OM}. If u_* is an underestimate by 10%, then this would increase our estimate of Z_{OM} to 1.47 m.

We then calculated the conductance for heat in (3) from

$$g_H = \frac{u_* \theta_*}{(T_c - T_{air})} = u_* \Big/ \left\{ \frac{1}{k} \left[\ln\left(\frac{Z - D}{Z_{OH}} \right) - \psi_H\left(\frac{Z}{L} \right) \right] \right\}. \quad (9)$$

We assumed $Z_{OH} = Z_{OM}$ and simply substituted 7.75 from (8) for the first term in the denominator.

The two Monin–Obukhov ψ functions for unstable conditions were used in the form (Paulson 1970; Dyer 1974)

$$\Psi_M = 2 \ln[(1 + x)/2] + \ln[(1 + x^2)/2] + \frac{\pi}{2}\left(1 - \frac{4}{\pi} \tan^{-1} x \right), \quad (10a)$$

$$\Psi_H = 2 \ln[(1 + x^2)/2], \quad (10b)$$

where

$$x = (1 + 16(Z/L_v))^{1/4}. \quad (11)$$

c. Estimates of error

One parameter that is important to our estimate of g_{veg} is the aerodynamic conductance, g_H. There are two important sources of error. Biases in u_* have been mentioned: a low bias would decrease the numeric value in (8) and increase g_H, as well as increase the second u_* value in (9). The second error source is the assumption of $Z_{OH} = Z_{OM}$. Many studies have concluded $Z_{OH} < Z_{OM}$, although the issue is not well resolved for the boreal forest (Sun and Mahrt 1995). A lower value of Z_{OH} than Z_{OM} reduces g_H, and increases $(T_c - T_{air})$, offsetting a likely low bias in u_*. In the composite datasets we shall use in the next section $(T_c - T_{air})$ reaches 2 K at high net radiation levels. Here T_c is a model aerodynamic temperature, which is not measured. Its relationship to observables such as a canopy radiometric temperature (T_{crad}) is discussed in Mahrt et al. 1997. At this spruce site however we have no measurement of canopy radiometric temperature. At the nearby NSA old jack pine site we do, and typical midsummer peaks in $(T_{crad} - T_{air})$ reach 2–3 K. This suggests that our estimates of g_H are reasonable. An order of magnitude reduction of Z_{OH} would increase our summer mean values of $(T_c - T_{air})$ to 5 K at high radiation levels.

3. Analysis of 30-min data

In this section we composite the 30-m data for the 3 yr 1994–96 to show the physical relationships that can be seen in the data. We will use a breakdown of the data into three broad seasonal classes: spring, defined here as before the soil melts at 10-cm depth; summer between soil melt and first frost; and fall after the first frost to the beginning of December. (Our ''spring'' class is rather broad as there are considerable periods when a key variable is missing: in 1995 it includes some data in February, while in 1996 it starts in March.) These seasons of homogeneous plant activity can be clearly seen in the analysis of the photosynthetic data in Goulden et al. (1997). From a climatic perspective, it is important that we understand the seasonal control on evapotranspiration, which we shall see is very large at these high latitudes, where the ground is frozen for many months of the year. All of the composites have been filtered to represent only unstable conditions (as discussed below), and we will provide the most detailed analysis of unfrozen ''summer'' conditions with air and soil temperatures >0°C. Naturally surface fluxes are largest (and the measurements are most reliable) during the unstable daytime hours, and the vegetative controls, which are of great climatic importance, are most important in the summer growing season.

a. Filtering of the data

There are about 46 000 30-min data segments in the 3-yr period, of which only 12 700 have upward sensible and latent heat fluxes and negative Monin–Obukhov length,

$$SH > 0, \qquad LH > 0, \qquad L_v < 0,$$

corresponding to unstable conditions. We selected these as our first filtered set to solve (3) and (4) and the Monin–Obukhov Eqs. (9)–(11) for unstable conditions. After then removing records with key missing parameters (air and soil temperature, humidity, wind speed, and PPFD), we were left with 8700 30-min segments. We also filtered out a small number of records (about 120) when it was actually raining during the 30-min period.

However, at low fluxes and near zero Monin–Obukhov length, solutions for R_{veg} are less reliable and sometimes diverge, so we tightened the filters to

$$SH > 20 \text{ W m}^{-2}, \quad LH > 10 \text{ W m}^{-2}, \quad L_v < -10 \text{ m}.$$

Finally we filtered out a few outliers by imposing limits on the derived R_{veg} and g_{veg} of

$$0.0001 < g_{veg} < 1 \text{ m s}^{-1}$$

$$0.1 < R_{veg} < 1000 \text{ s m}^{-1},$$

leaving 6090 data points, roughly 3000 h of data, extracted from a 3-yr period, 1994–96. These we divided into the three broad seasonal classes defined above: the spring class (before the soil melts at 10-cm depth) has 1264 data points. Summer (between soil melt and first frost) has 4110 points, all with both soil and air tem-

perature above freezing, and fall (after the first nighttime frost to the beginning of December) has 716 points, of which 595 have unfrozen soil at 10-cm depth. The summer dataset is the largest and will be analyzed most extensively.

Smaller subsets, for example, for individual years, show qualitatively similar results, so we believe we have enough data to draw conclusions. This is the great benefit of a long dataset. However, we cannot give reliable error estimates on the graphs using the composite approach, since there are so many independent variables. We will show a few representative standard deviations, but in many cases, they are not very informative, as in addition to the sampling error in each 30-min mean (of perhaps 30% in the fluxes under unstable conditions), there are many other physical variables in each subsample, some of which have a large diurnal variation. In section 5 we will use multiple linear regression to show that over 60% of the variance in our derived bulk vegetative resistance for the summer period can be explained in terms of physical variables.

b. Wet surface and cloud indices

As an aid in stratifying the data we constructed two important indices: one to represent the storage of water on the surface, particularly in the moss layer, and a second as an indicator of cloudy conditions or diffuse radiation falling on the forest. Both these physical processes appear to have a significant impact on evapotranspiration from the forest.

Other studies (Price et al. 1997) have shown that canopy interception and storage in the moss layer play an important role in the evaporation from the boreal forest system. They found that canopy interception over a summer season was 23% of precipitation, and moss storage and evaporation was 23% of the total throughfall. Since we do not have measurements of the canopy water storage or moss water content at this spruce site for the period 1994–96, we have computed a rather simple *wet surface index* (WS) based on the rainfall on preceding days, as follows. We assume the combined moss and canopy has an average maximum storage of 5 mm of water, and in the absence of rain this storage falls 1 mm day^{-1} (either by evaporation or drainage). After daily total rain of 1–5 mm, we set this WS to an integer value of 1–5 and decremented it by 1 for each following day that had less than 1 mm of rain. Rainfalls above 5 mm were given the index 5. The index remained constant on a subsequent day, if daily rainfall was 1 mm, and was incremented again for daily rainfalls of 2–5 mm (or more). This WS gives a qualitative indication of the surface water storage. Zero means that for at least 5 days, less than 1 mm of rain fell, and the moss layer (as well as the canopy) is probably quite dry. Index 5 means that at least 5 mm fell the preceding day, and the surface including the moss layer is likely to be quite wet. Indices 1–4 represent intermediate conditions of either less rainfall, or dry downs from rain events. We shall find that this index, though qualitative, gives very useful stratifications of the data, which show the systematic impact of surface water storage on evaporation, and the relatively long timescale of several days for the dry down of the moss layer, which is of climatic importance. During and immediately following rainfall, evaporation from the wet canopy is likely to be high, but we were not able to separate the canopy and the moss layer storage and evaporation in this analysis.

The *cloud index* (CX) gives a useful indication of whether the incoming radiation is direct or diffuse. Goulden et al. (1997) showed that gross photosynthesis was 50% higher at the *same* incoming radiation level under cloudy skies than under sunny skies, because of the larger proportional contribution of shaded surfaces to photosynthesis. They used the ratio

$$R_{\mathrm{PPFD}} = \mathrm{PPFD\ (below\ canopy)/PPFD\ (above\ canopy)}, \tag{12}$$

which is bimodal, to distinguish sunny and cloudy conditions—defining $R_{\mathrm{PPFD}} < 0.12$ as sunny conditions and $R_{\mathrm{PPFD}} > 0.12$ as cloudy conditions. Using the same threshold, we defined a CX, CX = 0 for sunny conditions and CX = 1 for cloudy conditions. We will show in sections 4f and 5 that vegetative resistance was significantly less under cloudy conditions, so that evaporation from the forest is higher under diffuse light, even for the *same* incoming radiation. In the appendix we shall show that the surface energy balance closure is improved under cloudy conditions.

c. Dependence of evaporation on season, incident radiation, temperature, and wet surface index

Figure 4a shows LH plotted against incident PPFD, with a breakdown of the data into the three broad seasonal classes. The data has been simply averaged in 300 μmol m^{-2} s^{-1} bins centered on the values shown. In the summer dataset, a mean PPFD of 1650 μmol m^{-2} s^{-1} corresponds to near-full sun at local noon and a mean R_{net} of about 590 W m^{-2}. We show some representative standard deviations: they are quite large as the meteorological parameters vary, in addition to the sampling error in each 30-min mean. Spring LH flux, when the soil is frozen, is very low and increases little with PPFD. Consequently at high radiation levels, the SH flux is high, which leads to deep boundary layers over the forest in spring. The LH flux in fall after frost and its dependence on PPFD, while larger than in the spring, is considerable less than in summer.

Figure 4b is a further breakdown of just the summer data. The heavy solid line is LH for all the summer data, and the dashed lines show the partition into three air temperature ranges (at 29 m). Even in summer, the increase of evaporation with increasing radiation and temperature is relatively weak. The increase of evaporation is controlled largely by the vegetative resistance in Eq.

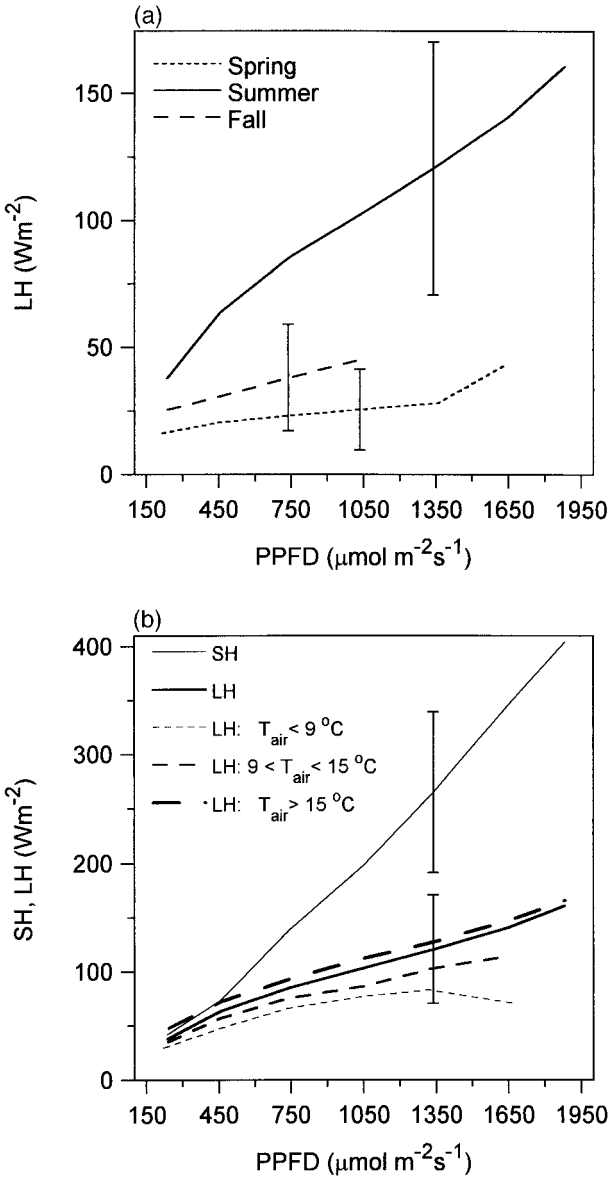

FIG. 4. (a) Dependence of LH on incident PPFD for spring (frozen ground), summer, and fall (after frost). (b) SH and LH (in three air temperature ranges) as functions of PPFD.

(6b), which is much larger than the aerodynamic resistance (see section 4), so that SH increases faster than LH (light solid line) at high light levels.

Figure 5 shows the large effect of a wet surface on summer evaporation for different light levels. For our highest WS, WS = 5, evaporation is about 50% higher than when the moss is dry. The variation with surface wetness is larger than the variation with temperature shown in Fig. 4b. Clearly the surface reservoirs including the moss are playing an important role in water storage and evaporation in the ecosystem. This is consistent with measurements at a nearby site at Joey Lake,

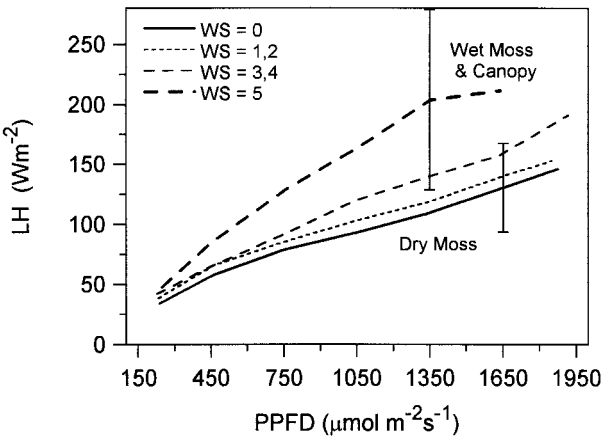

FIG. 5. LH as a function of PPFD for different ranges of a wet surface index.

Manitoba, where Price et al. (1997) found that the sum of canopy interception and moss evaporation was about 41% of the precipitation, corresponding to 0.6 mm day^{-1}, or about 35% of the measured midsummer evaporation rate at the black spruce site of 1.7 mm day^{-1}.

d. Dependence of evaporative fraction on temperature and incident radiation

Figure 6 shows evaporative fraction (EF), defined as

$$EF = LH/(LH + SH) \quad (13)$$

as a function of PPFD. The solid curve is an average of all the summer data (4110 points). The dashed and dotted curves further break the summer data into three ranges of air temperature as shown. Figure 6 shows that EF *decreases* with incoming radiation at all temperatures. The fact that the solid curve for all the data has less of a slope and crosses the dashed curve reflects the

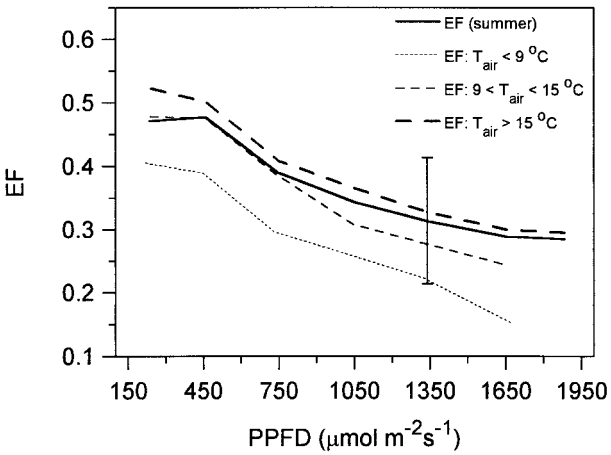

FIG. 6. EF as a function of incident PPFD in three air temperature ranges.

fact that temperature increases at higher PPFD levels on average. This illustrates why careful stratifications of the data are needed to separate the underlying dependencies. This partition by temperature shows that the fall of EF with light level is true at all temperatures. The increase of EF with temperature comes primarily from the dependence of saturation mixing ratio and evaporation on temperature through the Clausius–Clapyron equation. Standard deviations about the sample mean are of order 0.1 as shown. The fall of EF with increasing light level comes from the fact that the LH flux is strongly constrained (see Fig. 4b). To interpret the physical constraints on evaporation further, we will derive a bulk vegetative resistance.

4. Dependence of forest vegetative resistance on physical variables

Using the simple bulk vegetation model discussed in section 2a, we calculated a bulk vegetative resistance to evaporation for the spruce forest for unstable conditions for each 30-min time average. After filtering the data, as discussed in section 3a, we now show stratifications of the dependence of this bulk vegetative resistance on observed variables. Since we are dealing with data from an individual site, and the flux data itself has probable biases as well as scatter, we would caution that the relative variation of R_{veg} with different variables is likely to be more useful than the absolute value of R_{veg} in evaluating whether model land surface parameterizations have a realistic representation of the processes we observe at this black spruce forest site. Figures 7–10 are all for the summer dataset.

a. Dependence on PPFD and RH

Figure 7a shows the dependence of R_{veg} on incoming PPFD for ranges of relative humidity (RH) for the summer data. The heavy solid curve is the average of all the data for all RH. It suggests very weak dependence on PPFD. However if we bin the data by RH, the picture changes, because the decrease of vegetative resistance with increasing RH is very marked. For low RH $< 30\%$ (solid line), R_{veg} is high, and falls at high light levels, that is as expected, the forest evaporates water more readily when high light levels drive photosynthesis. As RH increases, R_{veg} decreases and the fall with increasing light level decreases as well. For nearly saturated air (RH $> 80\%$), the resistance to evaporation is low, and falls weakly with increasing light. The standard deviations show that this dependence on RH is so large that the distributions at high and low RH are largely nonoverlapping.

Figure 7b shows the similar pattern that we get by partitioning by vapor pressure deficit (VPD). Again the heavy solid curve is for all the data. These stratifications are similar but not formally equivalent, since

$$\mathrm{VPD} = \mathrm{SVP} \cdot (1 - \mathrm{RH}),$$

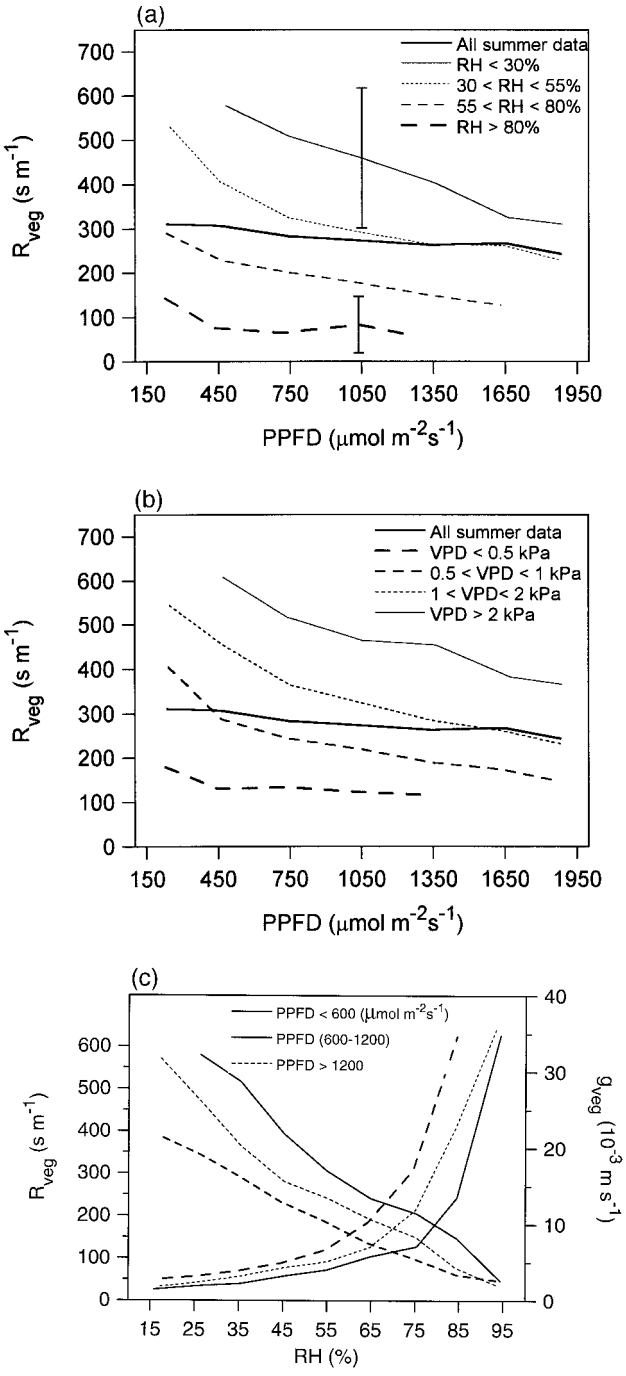

FIG. 7. (a) Dependence of vegetative resistance (R_{veg}) on incoming photosynthetic radiation (PPFD) for RH ranges. (b) As in Fig. 10a but in VPD ranges. (c) The R_{veg} (left-hand scale) and vegetative conductance (g_{veg}: right-hand scale) for three light levels, binned by RH.

where SVP, the saturation vapor pressure, is an exponential function of temperature. We shall use RH here to stratify the data and then look at the temperature (T) dependence for different RH (see Fig. 11 later). We

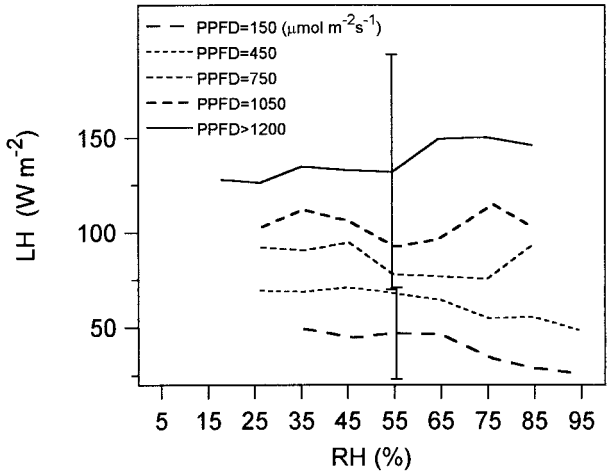

FIG. 8. LH as a function of RH for different light levels, showing weak dependence.

found that RH and T explain significantly more of the variance in R_{veg} than do VPD and T (see section 5).

Figure 7c shows both R_{veg} (left-hand scale) and average vegetative conductance, g_{veg}, on right-hand scale, for three light levels, binned by RH. At high humidities, g_{veg} increases rapidly, while R_{veg} has a quasi-linear dependence on RH. For this reason also we will use R_{veg} and RH in our linear regression analyses (see section 5). Note however that the average of R_{veg} shown in Fig. 7c does not correspond exactly to the average of its reciprocal g_{veg}, because of the scatter of the distribution. Typically

$$\overline{R_{veg}} > 1/\overline{g_{veg}}$$

and the difference increases from about 5% for high $\overline{R_{veg}}$ to about 50% for the low values of $\overline{R_{veg}}$.

The effect of this strong dependence of R_{veg} on RH shown in Fig. 7c is that evaporation is very *insensitive* to $[q_s(T_c) - q_{air}]$ in Eq. (4) and to RH. Figure 8 shows LH as a function of RH for different light levels for the summer data, showing this weak dependence. It appears that the forest has a tight physiological control on its transpiration rate, so that evapotranspiration *does not increase as RH goes down.* This insensitivity of forest evaporation to RH is of considerable climatic importance. It is interesting to note that the weak maximum at high RH for the upper curve, corresponding to high incoming light, corresponds to a prevalence of days with a wet surface. This very weak dependence of LH on RH is consistent with the finding of Goulden et al.

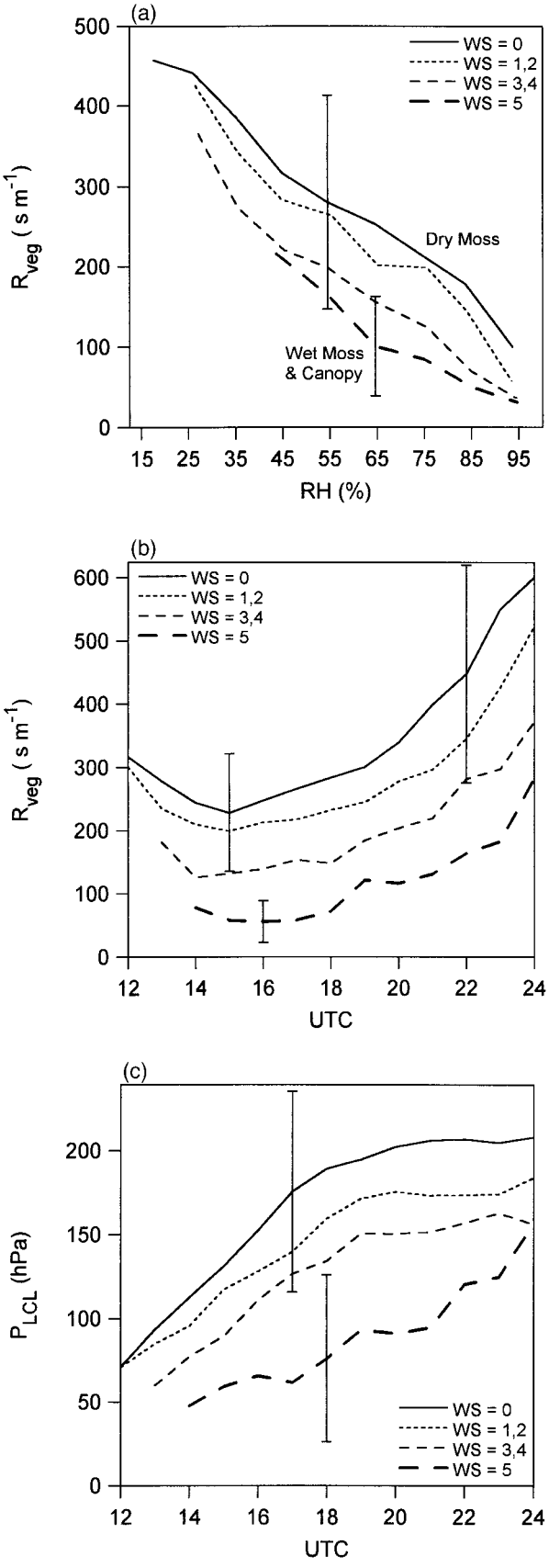

→

FIG. 9. (a) The R_{veg} for the forest system in summer as a function of RH and wet surface index (WS). (b) Diurnal variation of R_{veg} in summer, stratified by WS. (c) Diurnal cycle of P_{LCL}, the pressure height to the LCL, stratified by WS.

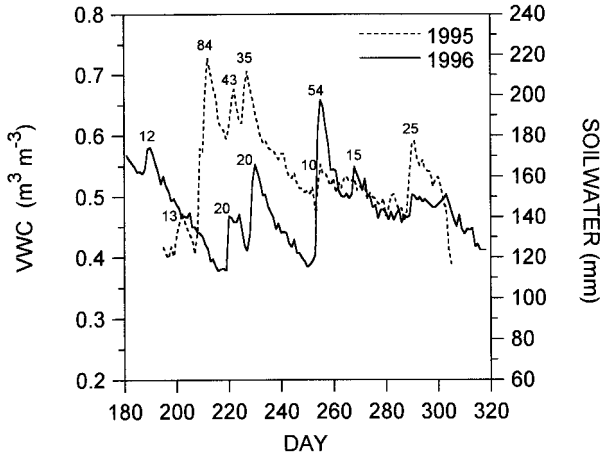

FIG. 10. Mean VWC (on left-hand axis) for 0–30-cm layer for Jul–Oct 1995 and 1996. The total water storage in this layer is shown on the right-hand axis.

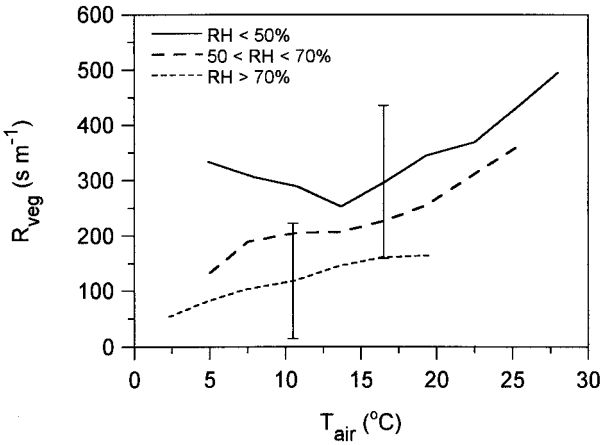

FIG. 11. Dependence of R_{veg} on air temperature and RH for summer data.

(1997) that gross photosynthesis is only weakly dependent on VPD.

b. Dependence on wet surface index

Figure 9a shows how R_{veg} for the forest system is a strong function of the WS. The solid curve corresponds to a dry surface, and the dashed and dotted curves to higher WSs. When the surface is wet, the mean ''vegetative resistance'' is more than halved at higher RH (in fact the evaporation from the wet moss is not stomatally controlled). The corresponding PPFD distribution (not shown) is quite similar across all wet surface indices, so this is not an effect of different light levels.

c. Diurnal variation as a function of wet surface index, and feedback to the boundary layer

Figure 9b illustrates the large diurnal variation of R_{veg}. There is a midmorning minimum of R_{veg} (a consequence of RH falling and PPFD rising) and a late afternoon maximum for all values of the WS (local noon is 1800 UTC). With a WS = 5, the computed midmorning ''vegetative resistance'' is a *factor of 4* lower than when the moss is dry. This is a larger difference between wet and dry surfaces than in Fig. 9a because the mean RH is much higher on days with a wet surface. Note that the error bars in Fig. 9b are smaller in a relative sense (and a little more meaningful) than in the preceding Fig. 9a, which does not stratify out the large diurnal variation. Evaporative fraction at local noon increases uniformly from only 0.3 for the dry surface days to 0.5 for the WS of 5 (not shown).

As over grassland sites (Betts and Ball 1995, 1998), this large difference in the surface resistance to evaporation (which leads to a difference in EF) directly influences the mean diurnal cycle of RH, and consequently the lifting condensation level (LCL). Figure 9c shows the diurnal cycle of P_{LCL}, the pressure height to the LCL of near-surface air (at 29 m), stratified by WS. A uniform decrease of LCL (and with it mean cloud base) with increasing surface wetness is visible. The mean LCL is over 100 hPa lower on the subset of days when the surface is very wet. This is the important climatic mechanism by which the resistance to evaporation from the surface feeds back on the boundary layer (BL) depth and the convective cloud field. It has no parallel over the ocean, where water is freely available for evaporation. A small part of the lower P_{LCL} in Fig. 9c can be attributed to decreases in the incoming photosynthetic radiation, which falls from 1370 μmol m^{-2} s^{-1} to 970 μmol m^{-2} s^{-1} at local noon as the WS increases from 0 to 5, presumably because cloud cover increases.

d. Dependence on soil water

For the second half of the measurement period (13 July 1995 onward), we have at five levels (7.5, 22.5, 45, 75, and 105 cm) soil moisture measurements from an array of eight sets of TDR probes at the site (Cuenca et al. 1997). We used the upper two levels to generate a daily average value of soil moisture for the 0–30-cm layer, representative of the spruce root zone. Volumetric soil moisture values in this layer are high: generally in the range 0.4–0.7. Figure 10 shows the changes in this mean volumetric soil water (VWC, on the left-hand axis) for July–October 1995 and 1996. The increases of total water storage for this 0–30-cm layer (shown on the right-hand scale) for the major rain events are qualitatively consistent with the total rainfall for the event, shown in millimeters above or to the left of each peak. After major rain events, soil water storage in this 30-cm organic layer falls rapidly about 4–6 mm day^{-1} through drainage, considerably more than the daily evaporation of about 1.5–2 mm day^{-1} on sunny summer

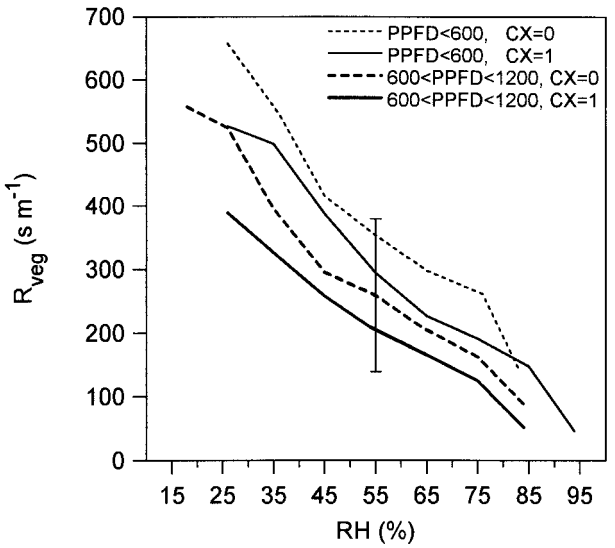

FIG. 12. Dependence of R_{veg} on cloud index in two PPFD ranges.

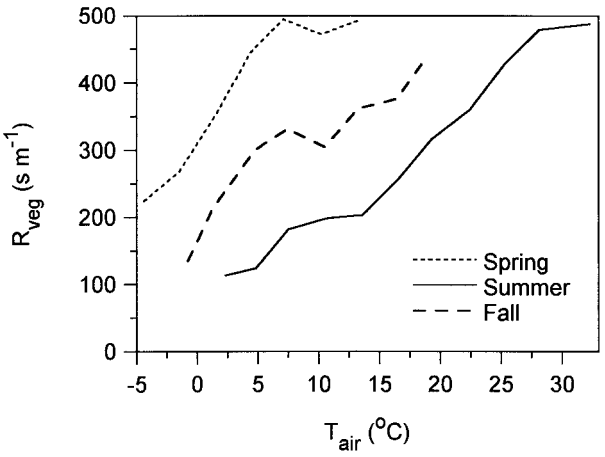

FIG. 13. Dependence of R_{veg} on air temperature for spring, summer, and fall datasets.

days. As discussed in sections 3c and 4b, both LH and R_{veg} show a large dependence on our WS after rain events. In contrast, any dependence of R_{veg} on 0–30-cm soil water is hard to detect, either by careful stratification of the data when the surface is dry (not shown) or by multiple linear regression (see section 5). This is a major difference between the boreal spruce forest and grassland, where soil water has a large impact on vegetative resistance and evaporation (Verma et al. 1992).

e. Dependence on temperature

Figure 11 shows the dependence of R_{veg} on air temperature (for the summer data with soil and air temperatures >0°C) in three bands of RH. The dependence on temperature is more subtle than that seen on PPFD, RH, and the WS. It appears that at lower humidities, there is a weak minimum of R_{veg} near 13°C, which may possibly have a physiological basis. At higher humidities, this minimum is not seen. At all humidities, R_{veg} increases at warmer temperatures. The dependence on PPFD is not a major effect in Fig. 11, as light levels increase only about 30% with increasing temperature (not shown).

f. Dependence on cloud cover

Figure 12 shows the further stratification of R_{veg} from Fig. 7c into sunny (CX = 0: dotted) and cloudy (CX = 1: solid) sky conditions (representing direct and diffuse solar radiation), for two ranges of PPFD. Here R_{veg} is less at all RHs under cloudy skies by about 50 s m^{-1}. Our regression analysis in section 5 will confirm this. This is consistent with the findings of Goulden et al. (1997) that photosynthetic uptake is greater under cloudy skies at the same radiation level, because the diffuse radiation penetrates the canopy more efficiently. The forest transpiration is thus higher when the incoming radiation is diffuse.

g. Effect of season and frozen soil

Figure 13 shows R_{veg} as a function of air temperature with the same stratification of the data into spring, summer, and fall as Fig. 4a. We see that the resistance to evaporation of the forest system at the same air temperature is a minimum in summer, and it is as much as 250 s m^{-1} higher on average, when the soil is frozen in spring (and the LH flux may include evaporation and sublimation of snow). In the fall after frost has reduced photosynthesis (Goulden et al. 1997), we see intermediate values of R_{veg}. There are other variable differences between these datasets. The spring dataset has a higher PPFD and lower RH: these effects on R_{veg} probably largely cancel (not shown). The fall dataset has a lower PPFD, which accounts for part of its higher R_{veg}. This large variation of R_{veg} with season is of great climatic importance.

h. Dependence on wind speed

In this simple bulk model for the vegetative control of evaporation, dependence on wind speed is only included though the dependence of the Monin–Obukhov framework on friction velocity u_*. Our simple model does not include an additional leaf BL resistance, and vegetative resistance is usually not treated as a function of wind speed. However, our derived R_{veg} shows a significant wind speed dependence, seen in Fig. 14. For low and high RH, R_{veg} (heavy solid and dotted lines) falls with increasing wind speed. We might ask whether this could be real, either at the canopy level (the leaf boundary layer) or increased evaporation from the wet

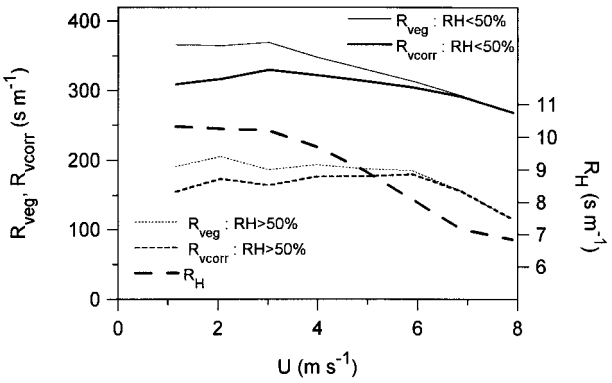

FIG. 14. Dependence of R_{veg} and R_{vcorr} on wind speed for high and low RH.

surface. However, even when the surface is dry, the same fall of R_{veg} with wind speed is seen (not shown). It is more likely however that part of this U dependence is a measurement problem at low wind speeds, as the energy balance residual falls sharply with increasing wind speed (see appendix). The fall of the much smaller aerodynamic resistance, R_H, with increasing wind speed, shown as heavy dashes on the expanded right-hand-scale, is as expected from Eq. (9).

The light lines, labeled R_{vcorr}, are computed after making a simple wind speed–dependent flux correction, since we believe that at low wind speeds the flux data may be underestimated. We supposed that the wind speed dependence of the residual was an error term and computed a linear energy correction (Corr) for $U < 7$ m s^{-1} of

$$\text{Corr} = 0.03(7 - U)R_{net}. \tag{14}$$

At $U = 1$ m s^{-1}, this energy correction is therefore 18% of R_{net} (see appendix). We then partioned Corr using EF into corrections to the SH and LH fluxes, to give corrected fluxes

$$\text{LH}_{corr} = \text{LH} + \text{EF} \cdot \text{Corr}, \tag{15a}$$

$$\text{SH}_{corr} = \text{SH} + (1 - \text{EF}) \cdot \text{Corr}. \tag{15b}$$

Then we recomputed a R_{vcorr} from these corrected fluxes, with one (significant) assumption that g_H is unchanged. That is, we did not correct u_*. The light solid and dotted lines in Fig. 14 are R_{vcorr}; they show a reduced dependence on wind speed. Perhaps the absence of a separate leaf BL resistance in our simple evapotranspiration model [Eq. (4)] might account for some of this remaining wind dependence of R_{vcorr}. The corrected value of R_{vcorr} are generally smaller than R_{veg}, because the residual correction increases the LH flux in Eq. (4), although the increase of SH increases ($T_c - T_{air}$) in (3) and therefore [$q_s(T_c) - q_{air}$], and this partly offsets the effect of increasing LH.

5. Regression analysis

Figures 7a, 9a, and 11–14 in the previous section show that R_{veg} is a function of PPFD, RH, wet surface index, air temperature, cloud cover, season, and possibly also wind speed. In these graphs, we can show only the dependence on two variables, and check that the others do not have large variations across the composites. The scatter in the data in the averages is large, as indicated by the sample error bars. This is to be expected in 30-min flux data, but the data sample of 3 yr is large enough that smooth trends can be seen in these composite averages. We can also have some confidence in these averages, as the patterns for individual years are qualitatively similar, although usually noisier. Multiple linear regression can show how much of the variance in the dataset can be explained in terms of linear dependence on selected variables.

We performed multiple linear regression on the same dataset of 4110 30-min flux values used for the summer composites in sections 3 and 4. The linear regression fit, using T, 1 − RH, PPFD, U, WS, and CX (cloud index) as independent variables explains 60% of the variance of R_{veg} giving (in s m^{-1})

$$\begin{aligned} &R_{veg}(T,\ 1 - \text{RH},\ \text{PPFD},\ \text{WS},\ \text{U},\ \text{CX}) \\ &= R_{veg}(1) = \underset{\pm 110}{170} + \underset{\pm 0.4}{9.0T} + \underset{\pm 12}{483(1 - \text{RH})} - \underset{\pm 0.005}{0.194\text{PPFD}} - \underset{\pm 1.1}{20.5\text{WS}} - \underset{\pm 1.2}{12.8\text{U}} - \underset{\pm 4}{53\text{CX}}. \end{aligned} \tag{16}$$

This regression equation is consistent with our earlier figures, showing the increase of R_{veg} with T, a strong increase with lower RH, and a decrease with higher PPFD, with increasing WS, cloud index, and increasing wind speed U (as discussed earlier in section 4h). The last term confirms that under cloudy skies (with CX = 1), R_{veg} is lower by 50 s m^{-1}. The explained variance is 2% lower if RH is replaced with VPD. As a predictor for R_{veg}, Eq. (16) has the limitation that it gives some negative values for high RH, high WS, and high PPFD. Indeed the dependence on some variables such as T in Fig. 11 appears nonlinear. The addition of some nonlinear terms, specifically T^2, WS · RH, and WS · PPFD, increase the explained variance to 62%, giving the equation fit

$$R_{veg}(2) = \underset{\pm 107}{228} - \underset{\pm 0.04}{0.43}(T - \underset{\pm 1.5}{6.3})^2 - \underset{\pm 1.2}{13.1}U + \underset{\pm 15}{552}(1 - \mathrm{RH}) - \underset{\pm 0.006}{0.219}\mathrm{PPFD}(1 - \underset{\pm 0.01}{0.085}\mathrm{WS})$$
$$- \underset{\pm 5}{61}\mathrm{WS}(1 - \underset{\pm 0.1}{0.7}\mathrm{RH}) - \underset{\pm 4}{55}\mathrm{CX}. \quad (17)$$

We have reorganized the nonlinear terms in (17) to show several features more clearly. The dependence on T is quadratic, with a minimum near 6°C. The fall of R_{veg} with PPFD is reduced when the surface is wet, suggesting that a smaller fraction of the evaporation is photosynthetically controlled. Here R_{veg} falls more with increasing WS at low humidities than at high humidities, also suggesting that the additional direct evaporation from the wet surface is not stomatally controlled.

We then repeated the regression analysis for R_{vcorr}, computed after applying the wind speed–dependent flux correction from Eqs. (14) and (15). This simple correction does reduce the dependence of R_{vcorr} on U, and it improves the variance explained to 63.5%, giving the regression equation

$$R_{vcorr}(3) = \underset{\pm 94}{173} - \underset{\pm 0.03}{0.41}(T - \underset{\pm 1.4}{7.1})^2 - \underset{\pm 1.0}{4.6}U + \underset{\pm 13}{508}(1 - \mathrm{RH}) - \underset{\pm 0.005}{0.201}\mathrm{PPFD}(1 - \underset{\pm 0.01}{0.09}\mathrm{WS})$$
$$- \underset{\pm 4}{58}\mathrm{WS}(1 - \underset{\pm 0.09}{0.68}\mathrm{RH}) - \underset{\pm 4}{50}\mathrm{CX}. \quad (18)$$

The fit is improved, with most of the coefficients being little changed, and there are now fewer negative values of R_{vcorr} (3). Considering that the individual data points are calculated from 30-min average fluxes, which are subject to appreciable sampling errors, we consider this explained variance of 63% to be quite good.

Figure 15 shows a plot of R_{vcorr} against R_{vcorr} (3), together with the 1:1 line, showing the goodness of fit and the unexplained scatter in the linear regression. We show only every other data point, as the figure is unreadable with the full dataset of 4110 points. Points with zero WS are dots, and each higher value of this index is indicated by a number, showing the strong role of the wet surface in determining R_{veg}. The clustering of 5's near the origin and their relative sparsity at high R_{vcorr} is apparent. There are still a few negative values of R_{vcorr} (3). These are almost all points with a high WS and a high PPFD. The regression also does not fit well the points with very high vegetative resistance, when evaporation is low. Recall that we have already filtered out all data points with $R_{veg} > 1000$ s m^{-1}. If we filter the dataset more severely at high R_{veg}, the regression fit improves a few percentage points (not shown).

For the subset of the data (2396 30-min samples) for which we have soil moisture measurements (after 13 July 1995), we added soil moisture as an independent variable in the multiple linear regression, but found that it increased the explained variance a negligible amount, even for the subset of the data when the surface was dry. The organic soil layer appears to be sufficiently moist that the variations of its water content have little impact on vegetative resistance. We also explored whether we could distinguish higher evaporation from a wet canopy (rather than wet moss) by labeling the first days after rainfall, but we found no significant improvement in the regression.

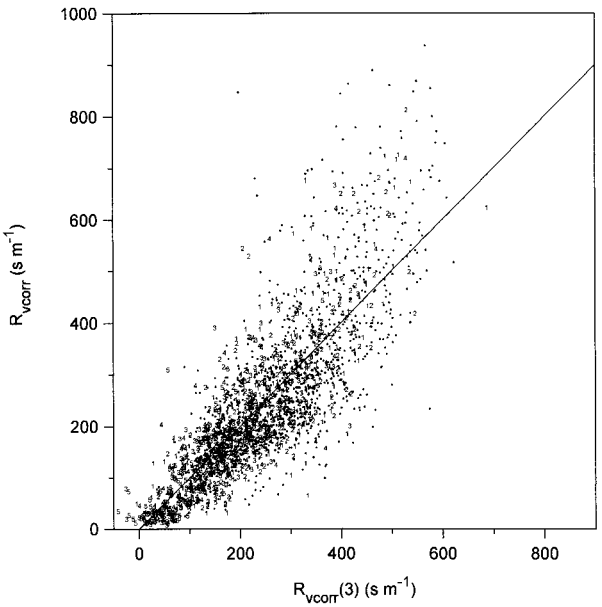

FIG. 15. Scatterplot of R_{vcorr} against R_{vcorr} (3) from multiple linear regression.

6. Conclusions

We have analyzed the surface energy balance over a boreal spruce forest using 3 yr of 30-min averaged data, collected during the 1994–96 BOREAS experiment, 40 km west of Thompson, Manitoba, to highlight the processes that appear important from a climatic perspective. Our intent has been to identify the physical processes that are apparent in the data, as a guide to their representation in model parameterizations of the boreal forest in climate and weather forecast models. The seasonal cycles of the surface sensible and latent heat differ markedly at these high latitudes. The sensible heat flux rises rapidly in spring as solar radiation increases, while evapotranspiration is small until the soil melts in May. The residual in the energy balance (we have no measurements of ground storage) has a marked seasonal as well as diurnal dependence. In spring when the ground and snow is melting, the residual reaches 30% of daytime net radiation.

We stratify the 30-min flux values to quantify the dependence of evaporation and vegetative resistance on air temperature, humidity and wind, incoming photosynthetic radiation, soil temperature, soil moisture (for a subset of the data), and two indices, CX and WS, representing cloud cover and the surface water reservoir. At the same incoming light levels, evaporation is much higher in summer than in spring when the ground is frozen. In the fall evaporation again falls after frost. Evaporation is much higher when the surface, which has an extensive moss layer, is wet. At all temperatures (in summer), evaporative fraction falls with increasing light level and net radiation, because of the high vegetative resistance of the forest system. We have calculated a bulk vegetative resistance during unstable conditions from the measured wind stress, SH, LH using a Monin–Obukhov surface model for the transfer coefficients. Using composites of about 2000 h of data during unstable conditions in summer, we find that the bulk vegetative resistance of the spruce forest system decreases with increasing light levels, decreases strongly with increasing RH, decreases as the surface gets wetter, and when the incoming solar radiation is diffuse under cloudy skies. We show the diurnal cycle of bulk vegetative resistance, stratified by WS. For all wet surface classes, R_{veg} falls to a midmorning minimum and then increases toward sunset. In midmorning R_{veg} is lower by a factor of 4 when the moss is very wet. As over grassland sites (Betts and Ball 1998), the lower surface resistance to evaporation greatly influences the diurnal cycle of lifting condensation and cloud base, which is much lower on days when the surface (including the moss) is wet. This is an important climatic feedback between the surface water reservoir and the depth of the subcloud layer. Even when the surface is dry, it is hard to detect any dependence of bulk vegetative resistance on soil moisture, because the root zone of the spruce forest has an organic soil with a high moisture content, near 50%. The reduction of vegetative resistance under cloudy skies at the same incoming radiation level presumably reflects the more efficient use of diffuse radiation by the canopy for photosynthesis, noted by Goulden et al. (1997). When the soil is frozen in spring, vegetative resistance is roughly doubled, and it rises again in fall after frost. The data also show a weak decrease of bulk vegetative resistance with increasing wind speed, but we believe at least part of this is due to flux underestimation at low wind speeds.

For this daytime summer dataset, multiple linear regression shows that 62% of the variance of our calculated bulk vegetative resistance can be explained by the variation of air temperature, humidity and wind, photosynthetic light level, a cloud index, and a wet surface index. A simple wind speed–dependent flux correction increases the explained variance to 63.5%. We give the regression fits for the uncorrected and corrected vegetative resistance as a function of observed variables. Some nonlinear terms suggest that the additional evaporation when the surface is wet is less subject to photosynthetic control, as might be expected.

An appendix explores the energy residual more fully. In spring when the ground and snow is melting, the residual reaches 30% of net radiation throughout the day, and presumably includes the large amount of energy going into the phase change of water. The summer daytime diurnal cycle of the residual falls steadily during the day as a fraction of the net radiation. This residual as a fraction of net radiation is much smaller under cloudy skies than sunny conditions. The reason is unknown, although it might be a measurement problem. The residual does fall with increasing wind speed and this may be instrumental, caused by a 10%–15% underestimate at low wind speeds of the surface fluxes measured by eddy correlation techniques.

Our results are representative of only a single site, but the physical dependencies they show for this dominant vegetation type in the boreal forest provide a semiquantitative check on forest vegetation models used in weather forecast and climate models. Some global forecast models, such as those at ECMWF and NCEP, do not represent all the dependencies that are clearly apparent in the data. The seasonal dependence, especially the effect of frozen soil in spring is of particular climatic importance, as is the large impact of the surface water storage reservoir on evaporation [which has been noted by other BOREAS investigators (Price et al. 1997)]. In addition, some vegetation parameterizations do not include the large RH dependence seen here in the data, which acts to stabilize the LH flux from the forest, across a wide range of conditions. The lower vegetative resistance under cloudy skies, which is apparent in the data, could also be of climatic significance.

Acknowledgments. The BOREAS analysis by AKB was supported by NASA under Grant NAG5-7377 and by NSF under Grant GA95-05018. The TF-3 data col-

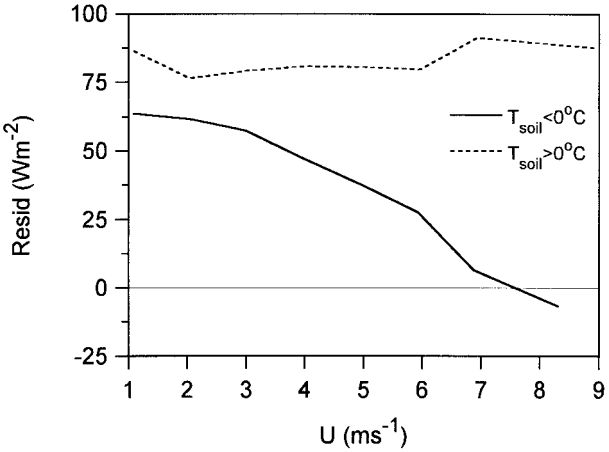

FIG. A1. Residual as a function of wind speed for frozen and unfrozen soil.

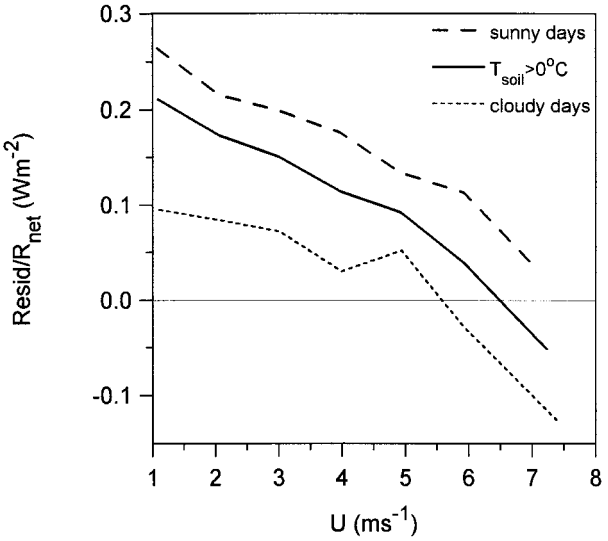

FIG. A3. As in Fig. A2 but for unfrozen soil data, partitioned into sunny and cloudy days.

lection was also supported by NASA. We are very grateful to R. Cuenca and S. Kelly for the soil moisture data and to Gordon Bonan for a helpful review.

APPENDIX

Closure of the Surface Energy Budget

The closure of the surface energy budget is an important issue in observational studies. As mentioned in section 1a, we have no accurate measurements of ground heat flux, as the heat flux plates did not survive the first winter. Goulden et al. (1997) discussed the residual in the surface energy budget, calculated as

$$\text{Resid} = R_{\text{net}} - \text{SH} - \text{LH}. \qquad \text{(A1)}$$

They noted that Resid/R_{net} = 0.18 on average, and this ratio reached a maximum in spring, when energy was used for the melt of soil and snow.

Goulden et al. (1997) also commented that energy closure improved with increasing wind speed. This appears to depend on whether the ground is frozen. We first filtered the 30-min data using

$$R_{\text{net}} > 30; \qquad \text{SH} > 20; \qquad \text{LH} > 10 \text{ W m}^{-2}$$

to select the data with upward heat fluxes and positive net radiation. There are 6141 rain-free 30-min averages in this filtered dataset (that also have measurements of air temperature and 10-cm soil temperature). We then averaged the 30-min data in 1 m s^{-1} bins of wind speed, and partitioned by mean soil temperature (at 10-cm depth) above or below freezing. Figure A1 shows that, when the ground is unfrozen, the residual falls sharply with increasing wind speed, but when the ground is frozen, the residual is both higher on average, and not a function of wind speed. The scatter in the residuals

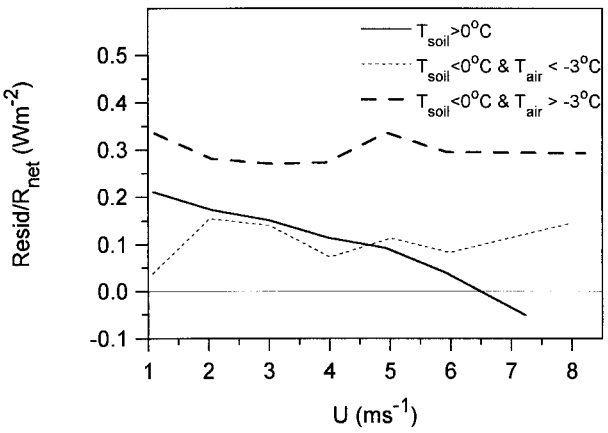

FIG. A2. Residual scaled by R_{net} as a function of wind speed for unfrozen soil, and frozen soil for two air temperature ranges.

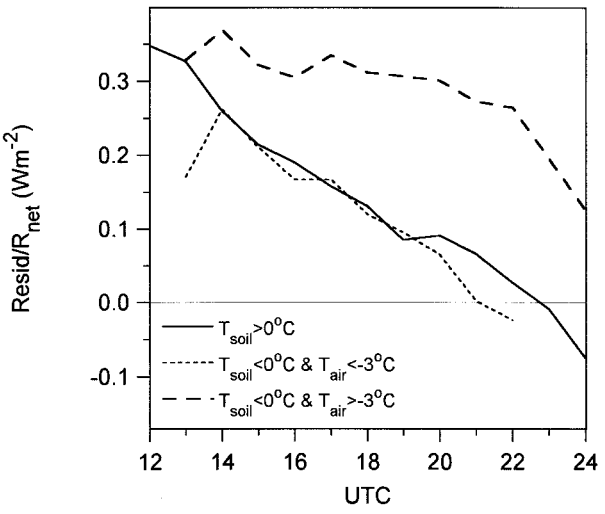

FIG. A4. As in Fig. A2 but showing the diurnal cycle.

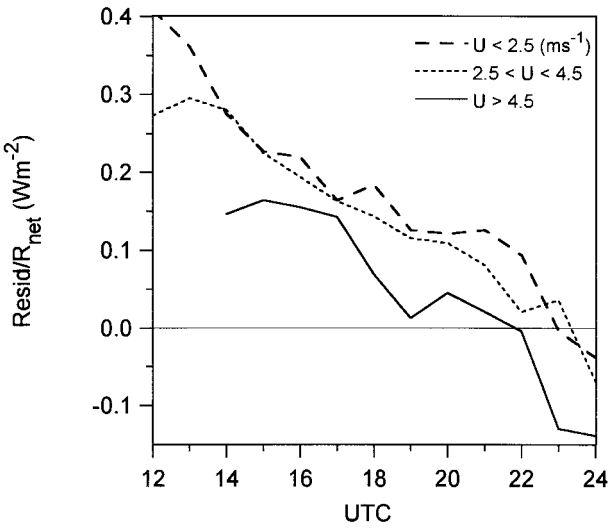

FIG. A5. Diurnal cycle of Resid/R_{net} for unfrozen soil, stratified into three wind speed ranges.

is large, perhaps not unexpectedly as these are 30-min data segments; the standard deviation about the mean line shown is 80–85 W m^{-2} at all wind speeds (not shown). Figure A2 shows the ratio Resid/R_{net}, with an additional stratification of the frozen soil according to air temperature, $T_{air} \leqq -3$°C. With frozen soil, and warm air temperatures, the Resid/R_{net} is now large: 0.29 ± 0.19, with apparently little variation with wind speed. When both soil is frozen and the air is cold ($T_{air} < -3$°C), Resid/R_{net} is much smaller, only 0.11 ± 0.25. With unfrozen soil, Resid/R_{net} decreases with wind speed and has an average of 0.125 ± 0.31. Some of the residual must be storage of energy in the soil and canopy. The increase in the residual at low wind speeds, when the soil is unfrozen, may be due to the eddy correlation measurements underestimating the surface fluxes (Goulden et al. 1997). At high wind speeds, when the ground is frozen, and the air warm, the high residual is probably due to transfer of energy to melt the ground, and the direct melting of snow by incoming radiation.

Figure A3 partitions the unfrozen soil data (solid line) into sunny (dashed) and cloudy (dotted) conditions, using the criterion defined in section 3b. Resid/R_{net} is a much smaller (by 10%–15%) under cloudy skies, although both have a similar wind speed dependence. The reason for this difference is unknown (it is much larger than the small additional photosynthetic uptake of energy). Calibration differences in the net radiometers under cloudy and sunny conditions are one possible reason, as are circulation changes under these different meteorological conditions.

The energy storage has a strong diurnal variation. Figure A4 shows the same partition of data by soil and air temperature as Fig. A2, but stratifies by UTC for the daylight hours (local noon is 1800 UTC). For both soil above freezing, and frozen soil and cold air temperatures, we see a similar pattern of a steady fall of Resid/R_{net} during the daytime. This is consistent with storage being large in the morning as the canopy and soil warms, and negative in the late afternoon, as the canopy starts to cool. However, the heavy dashed curve for frozen soil and $T_{air} > -3$°C shows only a weak diurnal trend, with a large Resid/$R_{net} \approx 0.3$. This again suggests that the melting of snow and ground soak up significant energy in the afternoon, when T_{air} is warm. Can we separate the wind speed dependence, which may be instrumental, from the strong diurnal cycle of storage? Figure A5 shows the diurnal cycle of Resid/R_{net} in three wind speed ranges for unfrozen soil. There does seem to be a trend of increasing residual with decreasing with speed. The daytime averages for the three curves for (Resid/R_{net} as a %, U m s^{-1}) are (18%, 1.8), (13%, 3.5), and (5%, 5.6). At high winds the average daytime storage is only 5% (although the scatter in the individual 30-min data values is large), while at lower wind speeds, Resid/R_{net} increases to 18%. We suspect that this may be an instrumental or sampling problem at low wind speeds, and the high wind speed diurnal variation is the more realistic.

Our conclusion is that, although the 30-min residual shows large scatter (with a typical rms of 80 W m^{-2}), one can see in large sample means the diurnal cycle of daytime storage and a large increase in ''storage'' when the ground (and snow) is (are) melting in spring. The residual does increase at low wind speeds by 10%–15%, which suggests that the surface sensible and latent heat fluxes may be biased low at low wind speeds. The residual is much larger under sunny skies than when it is cloudy, and we are unsure of the reason for this. There may be other residual errors, correlated with air temperature and humidity, but we cannot separate these from the daytime diurnal cycle variation of storage.

REFERENCES

Beljaars, A. C. M., P. Viterbo, M. J. Miller, and A. K. Betts, 1996: The anomalous rainfall over the United States during July 1993: Sensitivity to land surface parameterization and soil moisture anomalies. *Mon. Wea. Rev.*, **124,** 362–383.

Betts, A. K., and J. H. Ball, 1995: The FIFE surface diurnal cycle climate. *J. Geophys. Res.*, **100,** 25 679–25 693.

——, and ——, 1997: Albedo over the boreal forest. *J. Geophys. Res.*, **102,** 28 901–28 910.

——, and ——, 1998: FIFE surface climate and site-average dataset: 1987–1989. *J. Atmos Sci.*, **55,** 1091–1108.

——, S.-Y. Hong, and H.-L. Pan, 1996: Comparison of NCEP/NCAR reanalysis with 1987 FIFE data. *Mon. Wea. Rev.*, **124,** 1480–1498.

——, P. Viterbo, and A. C. M. Beljaars, 1998a: Comparison of the land–surface interaction in the ECMWF reanalysis model with the 1987 FIFE data. *Mon. Wea. Rev.*, **126,** 186–198.

——, ——, ——, H.-L. Pan, S.-Y. Hong, M. L. Goulden, and S. C. Wofsy, 1998b: Evaluation of the land–surface interaction in the ECMWF and NCEP/NCAR reanalyses over grassland (FIFE) and boreal forest (BOREAS). *J. Geophys. Res.*, **103,** 23 709–23 085.

Collatz, G. J., J. T. Ball, C. Grivet, and J. A. Berry, 1991: Physiological and environmental regulation of stomatal conductance,

photosynthesis and transpiration: A model that includes a laminar boundary layer. *Agric. For. Meteor.,* **54,** 107–136.

Cooter, E. J., M. B. Richman and P. J. Lamb, 1999: A climate change database for biological assessments in the southeastern United States: development and case study. *Climate Change,* in press.

Cuenca, R. H., D. E. Stangel, and S. F. Kelly, 1997: Soil water balance in a boreal forest. *J. Geophys. Res.,* **102,** 29 355–29 365.

Dickinson, R. E., A. Henderson-Sellers, P. J. Kennedy, and M. F. Wilson, 1986: Biosphere–Atmosphere Scheme (BATS) for the NCAR Community Climate Model. Tech. Note NCAR/TN-275+STR, National Center for Atmospheric Research, Boulder, CO, 69 pp. [Available from NCAR, P.O. Box 3000, Boulder, CO 80307-3000.]

Dyer, A. J., 1974: A review of flux-profile relationships. *Bound.-Layer Meteor.,* **7,** 363–372.

Goulden, M. L., J. W. Munger, S.-M. Fan, B. C. Daube, and S. C. Wofsy, 1996a: CO_2 exchange by a deciduous forest: Response to interannual climate variability. *Science,* **271,** 1576–1578.

——, ——, ——, ——, and ——, 1996b: Measurements of carbon sequestration by long-term eddy covariance: Methods and a critical evaluation of accuracy. *Global Change Bio.,* **2,** 169–182.

——, B. C. Daube, S.-M. Fan, D. J. Sutton, A. Bazzaz, J. W. Munger, and S. C. Wofsy, 1997: Physiological responses of a black spruce forest to weather. *J. Geophys. Res.,* **102,** 28 987–28 996.

Harden, J. W., K. P. O'Neill, S. E. Trumbore, H. Veldhuis, and B. F. Stocks, 1997: Moss and soil contributions to the annual net carbon flux of a maturing boreal forest. *J. Geophys. Res.,* **102,** 28 805–28 816.

Jarvis, P. G., 1976: The interpretation of the variations in leaf water potential and stomatal conductance found in canopies in the field. *Philos. Trans. Roy. Soc. London,* **273B,** 593–610.

——, and K. G. McNaughton, 1986: Stomatal control of transpiration. *Adv. Ecol. Res.,* **15,** 1–49.

——, J. M. Massheder, S. E. Hale, J. B. Moncrieff, M. Rayment, and S. L. Scott, 1997: Seasonal variation of carbon dioxide, water vapor, and energy exchanges of a boreal black spruce forest. *J. Geophys. Res.,* **102,** 28 953–28 966.

Jones, H. G., 1992: *Plants and Microclimate.* Cambridge University Press, 428 pp.

Larson, J. A., 1980: *The Boreal Ecosystem.* Academic Press, 500 pp.

Leuning, R., 1995: A critical appraisal of a combined stomatal-photosynthesis model for C_3 plants. *Plant, Cell Environ.,* **18,** 339–355.

Mahrt, L., Jielin Sun, J. I. MacPherson, N. O. Jensen, and R. L. Desjardins, 1997: Formulation of surface heat flux: Application to BOREAS. *J. Geophys. Res.,* **102,** 29 641–29 649.

Monteith, J. L., 1995: A reinterpretation of stomatal responses to humidity. *Plant, Cell Environ.,* **18,** 357–364.

Pattey, E., R. L. Desjardins, and G. St.-Amour, 1997: Mass and energy exchanges over a black spruce forest during key periods of BOREAS during 1994. *J. Geophys. Res.,* **102,** 28 967–28 975.

Paulson, C. A., 1970: The mathematical representation of wind speed and temperature profiles in the unstable atmospheric surface layer. *J. Appl. Meteor.,* **9,** 857–861.

Price, A. G., K. Dunham, T. Carleton, and L. Band, 1997: Variability of water fluxes through the black spruce (*Picea mariana*) canopy and feather moss (*Pleurozium schreberi*) carpet in the boreal forest of Northern Manitoba. *J. Hydrol.,* **196,** 310–323.

Sellers, P. J., Y. Mintz, Y. C. Sud, and A. Dalcher, 1986: A simple biosphere model (SiB) for use with general circulation models. *J. Atmos. Sci.,* **43,** 505–531.

——, and Coauthors, 1995: The Boreal Ecosystem–Atmosphere Study (BOREAS): An overview and early results from the 1994 field year. *Bull. Amer. Meteor. Soc.,* **76,** 1549–1577.

Smith, E. A., and Coauthors, 1992: Area-averaged surface fluxes and their time–space variability over the FIFE experimental domain. *J. Geophys. Res.,* **97,** 18 599–18 622.

Sun, J., and L. Mahrt, 1995: Relationship of surface heat flux to microscale temperature variations: Application to BOREAS. *Bound.-Layer Meteor.,* **76,** 291–301.

Verma, S. B., J. Kim, and R. J. Clement, 1992: Momentum, water and carbon dioxide exchange at a centrally located prairie site. *J. Geophys. Res.,* **97,** 18 627–18 639.

Wofsy, S. C., M. L. Goulden, J. W. Munger, S.-M. Fan, P. S. Bakwin, B. C. Daube, S. L. Bassow, and F. A. Bazzaz, 1993: Net exchange of CO_2 in a mid-latitude forest. *Science,* **260,** 1315–1317.